9-1-2014

Evaluation of the Thorax of Manduca Sexta for Flapping Wing Micro Air Vehicle Applications

Brian C. Cranston

Anthony N. Palazotto
Air Force Institute of Technology

Evaluation of the Thorax of Manduca Sexta for Flapping Wing Micro Air Vehicle Applications

Brian Cranston[1] and Anthony Palazotto[2]
Department of Aeronautics and Astronautics, Air Force Institute of Technology
Wright-Patterson AFB, Ohio, 45433-7765, USA
[1]PhD Candidate, Email: bccranston@gmail.com
[2]Distinguished Professor, Email: Anthony.palazotto@afit.edu

ABSTRACT

In the 1990's, DARPA awarded several contracts to companies to research, design, and construct a Flapping Wing Micro Air Vehicle (FWMAV). The tobacco hornworm hawkmoth (*Manduca sexta*) provides an excellent model from which to gather knowledge pertaining to the development of a Flapping Wing Micro Air Vehicle (FWMAV). One of the major challenges in design of a FWMAV is the energy demanding nature of low Reynolds number flapping flight. Therefore, an understanding of the power required by the flight muscles to actuate the wings is essential for the design of a FWMAV. The *M.sexta* wing/thorax mechanism was evaluated as a mechanical system in order to gain insight to the mechanical power required to produce the full natural wing stroke. A unique dynamic load device was designed and constructed to mechanically actuate the upstroke and downstroke of the *M.sexta* in order to achieve the full flapping motion. Additionally, the forces applied through the flight muscles were directly measured in order to attain the power requirements of the flight muscles simultaneously. The experiment yielded wing stroke values of + 60 and – 35 degrees, which is what is seen in nature during hovering. The DVM and DLM muscle groups were calculated to have a power density of 112 W/kg with the vehicle energy density being 2.5 W/kg. The power output requirement indicates the need for a lightweight and energy-dense power source/actuator combination for the development of FWMAVs.

NOMENCLATURE

AFIT	Air Force Institute of Technology
AFOSR	Air Force Office of Scientific Research
DAQ	Data Acquisition (board)
DARPA	Defense Advanced Research Projects Agency
DLM	Dorsolongitudinal Muscle
DoD	Department of Defense
DVM	Dorsoventral Muscle
FWMAV	Flapping Wing Micro Air Vehicle
fps	frames per second
IIT	Instrumented Indentation Testing
MAV	Micro Air Vehicle
M.sexta	*Manduca sexta*
RoM	Range of Motion
UAV	Unmanned Air Vehicle

1. INTORDUCTION

The following research study examined the flapping flight mechanism of a biological specimen, the Hawkmoth (*Manduca sexta*). In examining the Hawkmoth, the structure and function of the thorax/wing mechanism was evaluated for application to Flapping Wing Micro Air Vehicles. The

objective of this research effort is to quantify the power requirement for flapping flight of the Hawkmoth. The hawkmoth exhibits an indirect flapping mechanism, where in the muscles for flight is attached to a flexible segment of the exoskeleton. This mechanism functions utilizing a biological kinematic system to transmit the skeletal deflection to a wing deflection. Therefore, in order to quantify the power output of the moth the muscle/skeletal interaction must be investigated. The objective of this research effort is to quantify the power output of the main flight muscles (DVM, DLM) and power density during hovering flight conditions. To accomplish this goal a mechanical device was constructed that would actuate a euthanized *Manduca sexta* thorax such that the wings will flap through their natural frequency and flapping motion. The full flapping stroke was able to be reproduced in the *M.sexta* as well as instrumenting the vertical and longitudinal forces such that a power measurement was captured for the upstroke and downstroke. This power can then be attributed to each of the main muscle groups, the ventral and longitudinal muscles to attain a specific muscle power density for each group, which ideally would be the same if they are comprised of the same material.

Several different methods have been developed and tested with live and deceased *M.sexta* evaluating their muscle power output and more commonly used power density. Casey, in 1976 estimated the power density based on a calculated power input and an estimate of 20% efficiency. In 1983, Pennycuick estimated the power density of the flight muscle based on a known value of mitochondria in the muscle. By the 1990's, Stevenson and Josephson studied the ventral muscles utilizing a work loop method which was performed on partially disconnected muscles. Another work loop method experiment was performed by Tu in 2004, where he studied the longitudinal muscle group. In 2009 Zhao determined the power density using a numeric approximation for the inertial forces, and an experimental wing for the aerodynamic forces. The two were summed for the total power required for flight by the muscles. Lastly, in 2012 Hollenbeck utilizing some of the existing experimental set-up at AFIT estimated the power density for the ventral muscles using a unique dynamic load mechanism [9]. This research work built upon and improved the work performed by Hollenbeck by being able actuate the entire wing stroke and quantify more accurately and precisely the power required for the DVM and DLM muscle groups simultaneously. This is the first experiment technique known that successfully actuates and characterizes both muscle groups simultaneously and is truly unique.

2. BACKGROUND

2.1 M.sexta Selection/Investigation

The *Manduca sexta* also known as the Hawkmoth or Tobacco Hornworm Moth is an ideal specimen to study for its size, hovering ability, and remarkable flight stability. The *M.sexta,* according to aerodynamic calculations, has one of the lowest costs for hovering flight [1]. The *M.sexta* is described by M. A. Frye: 'This nocturnal forager hovers at individual flowers set against a spatially complex and dim visual background while maintaining stability in often turbulent winds" [2]. Beyond that, the *M.sexta* is widely used in current and past lab experiments, has ideal flight speed, wing span, wing loading, maneuverability, gust response, aspect ratio, flight Reynolds number and endurance. All of these attributes are critical to developing a successful FWMAV.

Figure 1. Dorsal view of *M.sexta* coloration (scale is in centimeters)

In addition to the exceptional flight characteristics of the *M.sexta,* it also exhibits an exoskeleton only seen in insects containing elastic proteins that enable the thorax to efficiently operate as a mechanical spring damper at resonance during flapping flight [3]. For wing actuation, the *M.sexta* has two fairly simple and easily isolated muscle groups. These are known as the dorsolongitudinal and dorsoventral muscle groups. For the purposes of this research effort the areas of interest that are the main focuses are the thorax and the muscle groups of the *M.sexta*.

2.2 M.sexta Flight Muscles

This research will focus primarily on the two major power producing muscles in flying insects, the dorsal longitudinal muscles (DLMs) and the dorsal ventral muscles (DVMs).

The DVMs are the elevator muscles that indirectly cause the upward movement of the wings in all insects. This occurs because when the DVM muscles are contracted, they pull down on the tergum (dorsal surface of the thorax), which moves the point of articulation of *M.sexta*'s wing down as well (Figure 2) [4]. In most insects (including *M.sexta*), the downward wing (depression) is caused indirectly when the DLMs contract; then, the center of the tergum becomes bowed upward, and this moves the upper wing joint upward and the wing flaps down (Figure 2C) [4]. *M.sexta* is amongst the largest of all flying insects. Their flight is powered by two sets of synchronously activated muscles in the thorax. The DLMs are the largest muscles in the moth, comprising 5-8% of the total body mass [5].

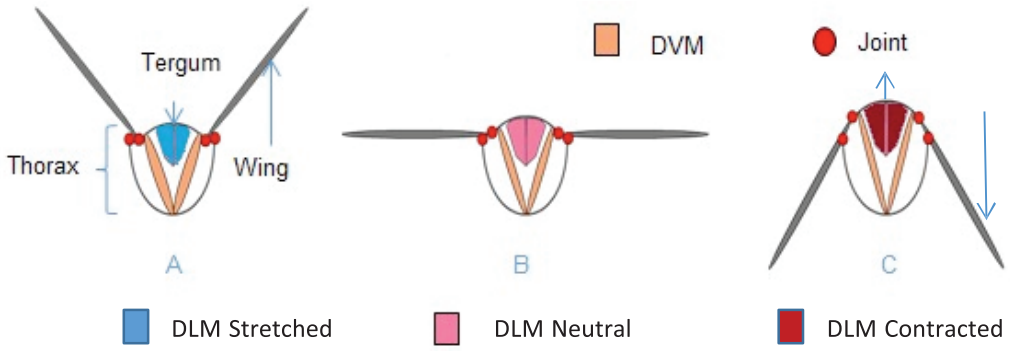

Figure 2. A cross-sectional view of a *M.sexta* thorax showing the primary flight muscles: A) DVM contracting, causing an up-stroke; B) DVM relaxing, while the DLM begins to contract; C) DLM contracting, causing a down-stroke

3. THEORY

3.1 Linkage Kinematics

For the purposes of the dynamic load experiment, it was necessary to develop an experiment that would actuate the thorax in both the vertical and longitudinal direction. In order to accomplish this, a linkage system was designed to actuate both the vertical and longitudinal compression with a single actuator.

Linkage systems are an assembly of bodies normally rigid to control forces and movement. The movement of the bodies or links is governed by geometric relationships. Connections between the links or bodies are known as ideally moving pivots. These pivots can be sliders, pinned rotations, and free moving pivots. The benefits in utilizing a linkage system is that it allows you to gain a mechanical advantage based on the design of the system and computable movements from each of the components in the system. These systems can have a vast array of pivot and link arrangements in order to achieve almost any desired movement for an output(s) [6].

The designed linkage system was decided to be a slider-crank mechanism and the equations relating the pivot and slider movement will be characterized below. The positional values of the pivot and slider are developed knowing three primary values: crank and shaft length and crank angle. Figure 3 shows a kinematic representation of a slider crank mechanism with the geometric relationships.

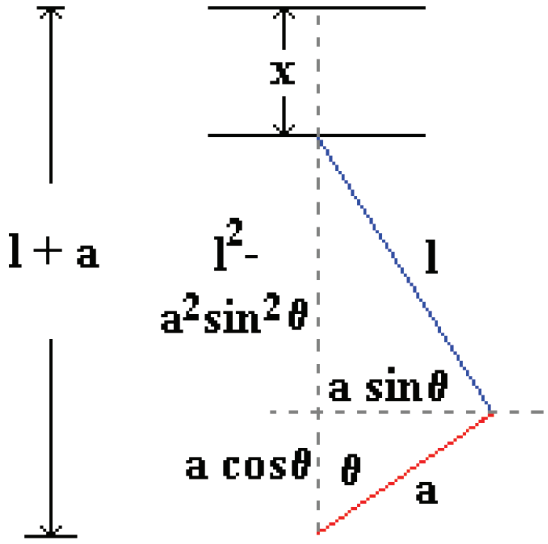

Figure 3: Geometric relationships of a slider-crank mechanism

The slider actuator displacement is denoted by equation 1.

$$x = a + l - [(l^2 - a^2 \sin^2 \theta)^{1/2} + a \cos \theta] \quad (1)$$

The pivot point joining the connecting rod (l) and the crank (a) has a horizontal displacement shown in equation 2.

$$y = a \sin \theta \quad (2)$$

In knowing the (l) and (a) lengths and the (x) displacement, the angle Θ can be back

calculated by solving equation 1 for Θ. With all of the unknowns established, all the kinematics of the slider-crank mechanism can be determined.

3.2 Specific Power Density

The specific power density and energy density are extremely useful values in determining the energetics of a material composition by weight. In general, higher values of power density are better than those of lower values. Typically, when investigating power densities of materials/fuels that are small, compact, and portable the main energy source is batteries. Commonly known battery types are those of the "dry cell" type, these include nickel-cadmium, nickel-zinc, nickel metal hydride, and lithium ion (ordered by increasing power density). This information is of importance when looking to compare the muscle power density of the specimen to available commonly used energy sources and actuators for FWMAV applications, which are mostly battery driven. The power density presented in the results section is computed from the force, displacement, and time data recorded using the dynamic load apparatus.

The first value to be computed from the experiment is work. Work can be calculated by computing the area under the force vs. displacement curve, or the integral of the force with respect to the corresponding displacement. This is illustrated in Figure 4. Work is also calculated by explicitly integrating the force-displacement area.

$$W = \int_{x1} F(x) d \quad (3)$$

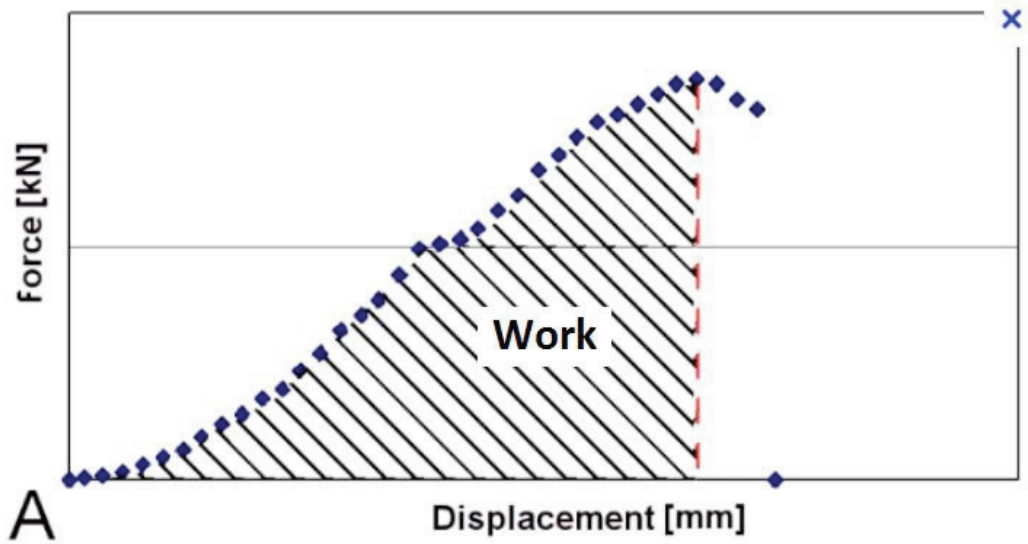

Figure 4: Example Force vs. Displacement plot, Work area under the curve

The trapezoidal rule was used in order to compute the area under the force vs. displacement curve.

After the work has been computed, the raw power quantity is simply the work divided by the amount of time the work occurred over. Power is in units of Watts or Joules per second.

$$P = \frac{W}{t} \tag{5}$$

From here the specific power density is the power computed from the work and time divided by the mass of the material/object that is performing the work. Hence, a large power density means the material can deliver large amounts of power for little weight.

Design, construction, implementation, and processing of the dynamic load experiment are detailed in the following section. The dynamic load experiment applied a vertical and longitudinal compressive force through the thorax at the natural flapping frequency. In compressing the thorax, the indirect flapping mechanism within was forced to actuate and flap the wings to full elevation and de-elevation. This technique of mechanically actuating the thorax is a unique technique.

4.1 Evaluation of the Slider-Crank Mechanism

The slider-crank mechanism operates under simple geometric relationships. Knowing the slider and crank length, and the crank angle, all of the positional quantities of the system can be solved for. Through kinematic and geometric evaluation of the mechanism, it was determined that the second pivot joint could be used to transmit the longitudinal force necessary to actuate the downstroke of the moth. At small crank angles, less than 20 degrees, the pivot displaces mainly in the longitudinal direction. The vertical displacement is shown to be small, the average slope being ¼, compared to that of the horizontal displacement.

Knowing that for small angles the horizontal displacement at the pivot is approximately four times larger than the vertical displacement; the designed linkage system proved to be sufficient for the proposed experiment. Apart from the pivot displacements, the other factor that needed to be satisfied for the system was the shaker displacement. The presented design produced a 1.08 mm displacement, which is well within the operational range of the shaker from zero- center. Other additional factors that constrained the linkage design were spatial considerations, such as pivot location constraints and lengths necessary to actuate the moth's rear phragma in the proper position. After several iterations, the linkage that produced the above pivot displacements was chosen to for the proposed experiment. The specifications of the linkage are shown in Table 1. The constructed linkage represented in SolidWorks is shown individually and connected to the system in Figure 5.

Table 1: Linkage Specifications

Linkage Specifications		
Crank length	9	mm
Slider length	8	mm

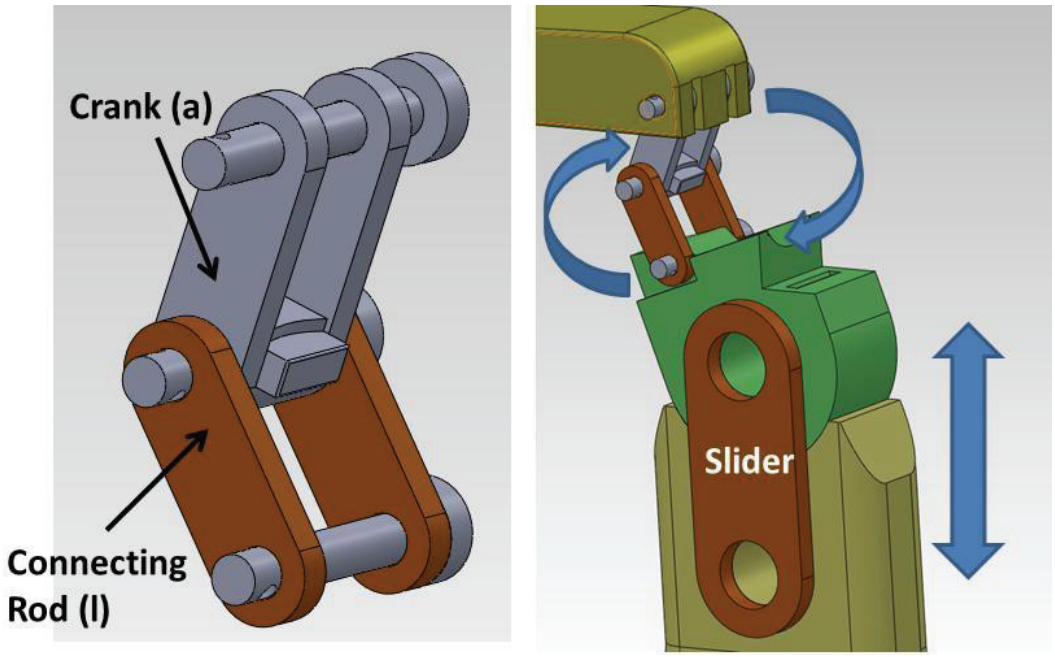

Figure 5: Slider-crank assembly as shown in SolidWorks

4.2 Dynamic Load Mechanism: Design and Construction

The constructed design was able to flap the wings at 28 Hz with amplitude of +- 55 deg to achieve a complete natural flapping stoke as well as force data for the respective compression directions.

When considering imposing a force that would actuate the dorsolongitudinal muscles, one needs to identify the attachment points of the muscles to impose the force. Quite differently than the ventral muscles, the longitudinal group lies between the head and the thorax. Therefore, in order to access the attachment points of the longitudinal muscles, the head and the thorax needed to be removed. Removing these muscles exposes the front and rear phragma, the attachment points of the muscle group. This exposure being necessary for actuation drove the design of the modified dynamic load platform.

After much iteration, a final working design was devised. The final design featured several components which were: a saddle mount, linkage mechanism, linkage mount extension, and longitudinal and vertical push rods with assembly. The set-up was modeled in a 3-D modeling program, SolidWorks, to attempt to work out design flaws and interferences within the system. The design is shown in Figure 6.

The construction evolved the original design, making it capable to perform both the upstroke and downstroke, while recording force measurements for both simultaneously. This system can fully replicate the full wing stroke of the hawkmoth as it flies in nature.

The smaller more intricate pieces were printed using an Objet Eden500V™ 3- dimensional printer. The material of the printed parts most closely resembles common ABS plastics. The larger flat pieces for the frame construction were made out of wood.

For the experiment, the specimen was moved vertically upward into the vertical push rod to produce the upstroke of the moth. At the same time the linkage pivot moves away from the rear of the specimen. As the mount moves downward, the pressure from the vertical rod is released and the linkage pivot swings forward into the rear phragma compressing the thorax horizontally against the longitudinal push

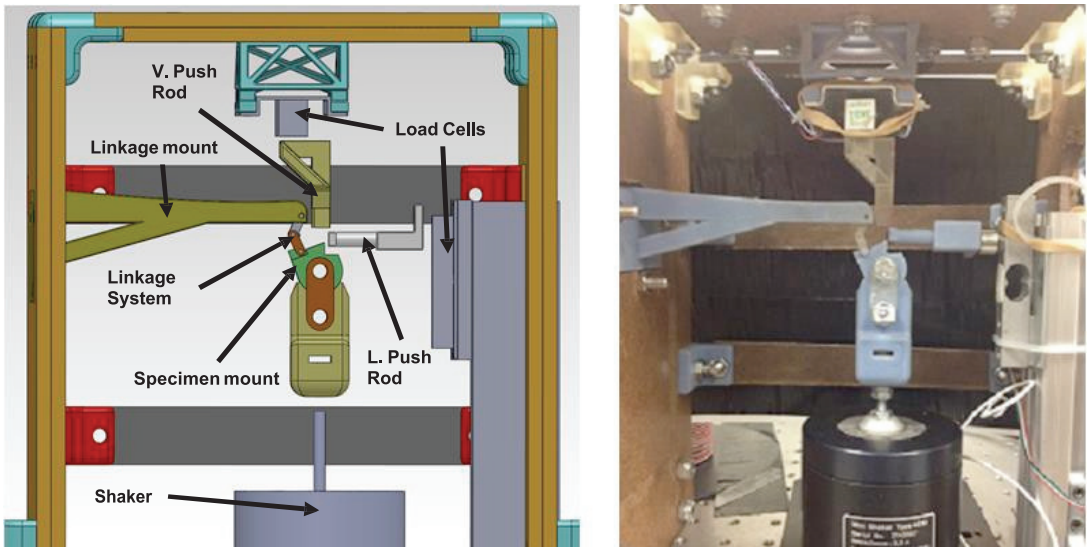

Figure 6: New build-up of the dynamic load experiment, accounting for vertical and longitudinal compression (The model depicts a gap between the push rods and load cells, in reality there were spacers in those locations for more accurate positioning. As shown in the image to the right)

rod producing a compression of the thorax in the horizontal direction yielding the downstroke of the wings. This process occurs 28 times a second (Hz). The mount is driven by a Brüel & Kjaer Mini Shaker Type 4810. The push rods were both analyzed using a finite element solver and were determined to be sufficiently rigid to produce an "infinite" stiffness thus requiring no adjustments for potential rod deformation.

4.3 Instrumentation and Data Acquisition

This section will detail all of the instrumentation utilized in order to achieve the desired specific power output results. The instrumentation is as follows, two 3 kg strain gauge cantilever beam load cells, a high speed camera, a laptop, and a data acquisition device (DAQ). The DAQ board used was a National Instruments USB-6251 BNC Data Acquisition device. The load cells were both powered through external power sources and their signals were sent through a designed and constructed amplifier board to yield a 0-5 Vdc signal to the DAQ. Before utilization of the load cells in the experiment, they required to be calibrated. The calibration process that was used involved taking a series of known weight values and placing them on the load cell and recording the signal voltage to the DAQ. The signal was observed utilizing the National Instruments *Measurements and Automation* software. The calibration yielded a linear relationship of mass to volts which was converted to force in Newtons for analysis of the power density.

The high speed camera that was used was a Dantec Dynamics NanoSense MkII high-speed video camera with a Nikon AF Nikkor 28 mm lens. The camera was triggered to begin to start recording at a specified frequency when the oscillatory signal sent to the shaker was executed. This ensured that each camera frame corresponded to a force signal from the load cell. Both the camera and load cells were set to record at 2500 Hz. This equal image to force data allowed for simpler processing and analysis. The software used to operate the camera was Motion Studio x64. The control hub for the signal acquisition and analysis was a laptop loaded with Windows 7, National Instruments DAQmx, MatLab R2011a x32, and Motion Studio x64. All of these pieces of software and their respective versions were necessary for the data acquisition portion of the experiment. A note of importance is that the 32 bit version of MatLab was necessary to communicate with the NI-DAQ drivers and components. A schematic of the communications connections of all of the above components is shown in Figure 7.

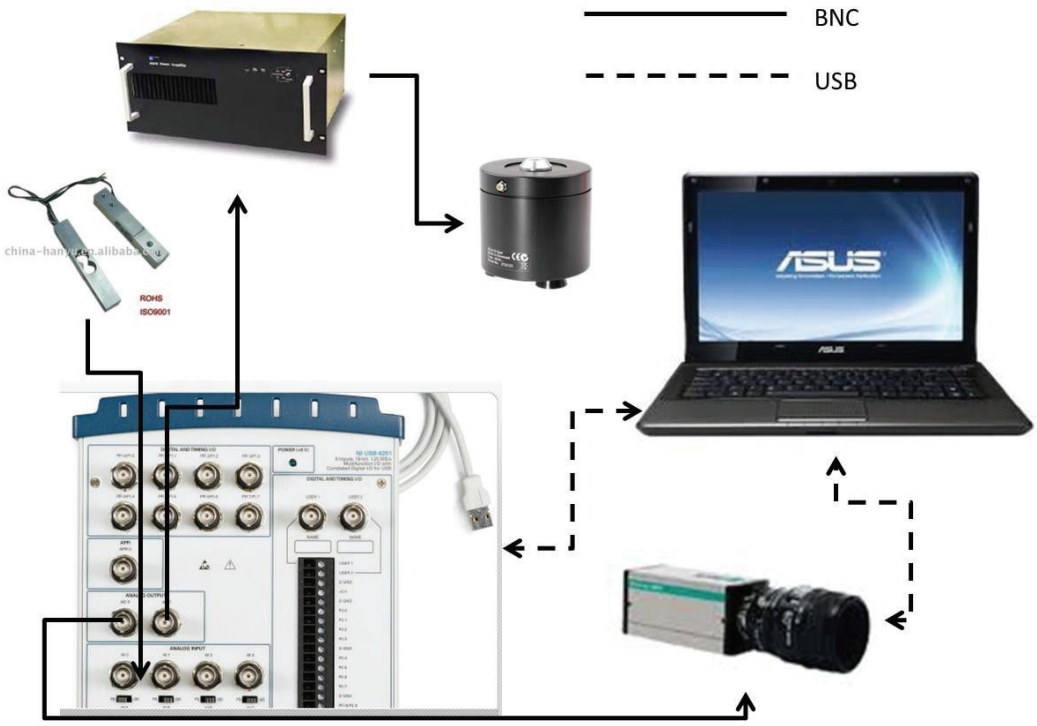

Figure 7: Wiring communications schematic of the experimental set-up

An image of the actual experimental set-up is shown in Figure 8. The communication chain between all of the components is as follows: The PC utilizing MatLab written code sends an input signal via USB to the NI-DAQ, the NI-DAQ sends two output signals, one to the camera and the other to the shaker amplifier, through the amplifier the shaker gets a sinusoidal forcing signal which drives the shaker and at the same time the camera is capturing images. After one second, 2500 data points are collected from the camera and each of the load cells and is sent back to the computers Matlab code for storage and analysis.

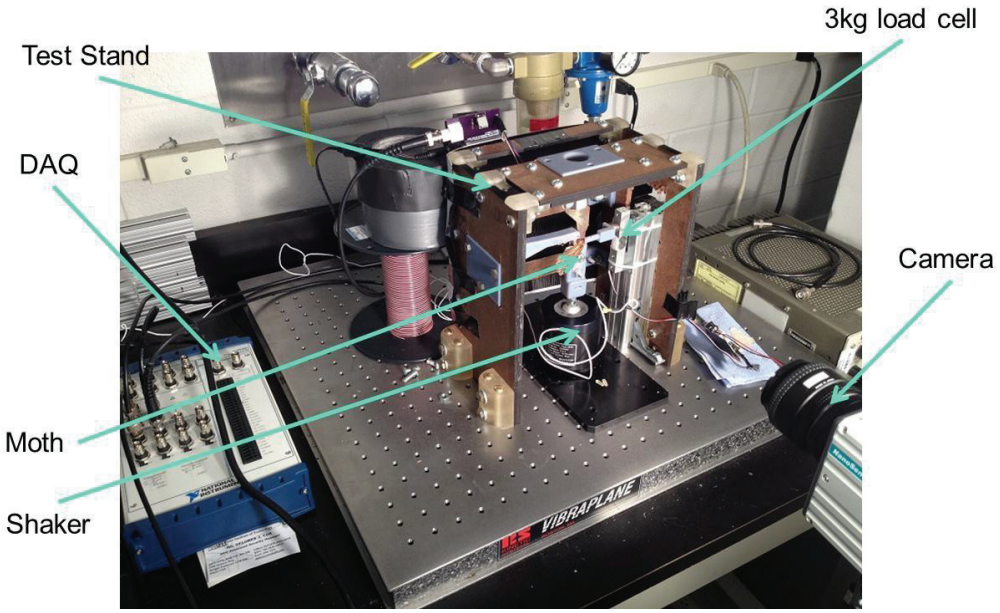

Figure 8: Experimental setup

4.4 Specimen Preparation

This section will detail how the specimen was prepared for the experiment and data collection. For the vertical compression test, the specimen was left mostly in its natural state apart from the euthanization and the legs being removed. This was possible because the area of required compression was on the top and bottom of the moth's thorax which is readily exposed. As mentioned earlier, in order to expose the attachment points of the longitudinal muscles the head and thorax would need to be removed to mechanically actuate the front and rear phragma. The specimen preparation and procedure was as follows:

1. Upon successful molting, the moth was removed from its habitat and transferred to a mesh cage that received light at all times, which inhibited the moths from flying.
2. While in the mesh cage, the moths were not fed any sort of diet, therefore their life span was fairly short (3-5 days). This meant that if the experiment was not ready for testing, the moths would be placed in a re-sealable plastic bag with a paper towel slightly moistened and placed into the freezer. This dampening of the cloth was noted to preserve the moth's integrity when thawed. However, all of the moths used for the results were fresh and not frozen.
3. When a moth was to be tested it was asphyxiated in a re-sealable plastic bag with a cloth dampened with acetone.
4. The moth was then weighed on a digital scale
5. Prior to testing is when the moths head, abdomen, and legs were delicately removed.
6. At this point the moth was now ready for testing and placed into the test fixture.

4.5 Experimental Procedure

This section will discuss the first process of the experiment, being the moth setup and live data acquisition. The moth, as prepared, was placed head towards the longitudinal push rod on the mount. A thin coating of dissection wax was placed between the moth and mount to reduce any slipping that might occur. At this point, the shaker mount assembly is disconnected from the linkage assembly to allow for ease of aligning the specimen on the mount. From here the mount is slid into place and the linkage assembly is pinned to the mount. Since the mount and linkage system were point designed, the mount needed to be in a single specific point vertically and horizontally for the linkage to work as designed. This being true, if any height adjustment was necessary to gain the desired spacing between the moth and the vertical push rod, the rod assembly was removed and the push rod was shimmed up or down with thin washers to accommodate for the spacing. The same technique was performed on the longitudinal push rod if adjustments were necessary. The moth as placed in the system is shown in Figure 9.

An LED spotlight was used to illuminate the area of the moth for the camera to have sufficient light for image capturing. The higher the frame rate of the camera, the lower the exposure time of each image, therefore a large amount of direct light was needed to provide the light source for each image. The camera was aligned, using a tripod, perpendicular to the longitudinal axis of the moth and roughly centered about the moth. Once everything was in place, the camera was set to receive a trigger signal and the signal communication code was executed through MatLab which began the test.

The overall goal is to be able to characterize the thorax deformation that the muscles provide to indirectly flap the wings. During the tests it was noticed that for the upstroke the wings were providing a significant inertia force on the load cell just after the thorax displacement; which made it difficult to extract the force that was purely input to the thorax. It was found through testing, that removal of the wings did not have a significant effect on the forces required to deform the thorax and actuate the wing hinge motion. Removal of the wings purely exposes the forces necessary to mechanically compress the thorax and therefore the work that the muscles would have to provide to compress the thorax.

In order to ensure that the wings still reached the full range of motion, the moth was tested with wings on and the video recorded by the camera was observed ensuring full wing displacement occurred. When satisfactory wing angles were achieved, the moth was left in the test rig in the exact position and the wings were removed using a pair of scissors.

The filtering of the load cell data was performed after the data was collected. The post processing process was to first run a Fast Fourier Transform on both load cell data arrays and determine the highest primary frequency of the signals.

Figure 9: Close-up view of the test apparatus with the specimen in place

The dominate frequency for both of the load cell responses was approximately 28Hz. This was determined by analyzing the FFT signals for the largest amplitude signal. This value was expected since the moth was flapped at that approximate frequency. The other peaks in the signal are harmonics of the 28 Hz signal. With the verification from the FFT that the signal of interest lays at or below 28 Hz the 2nd order low pass filter was set at a frequency of 30 Hz. Figure 10 shows an example of the filtered data versus unfiltered data.

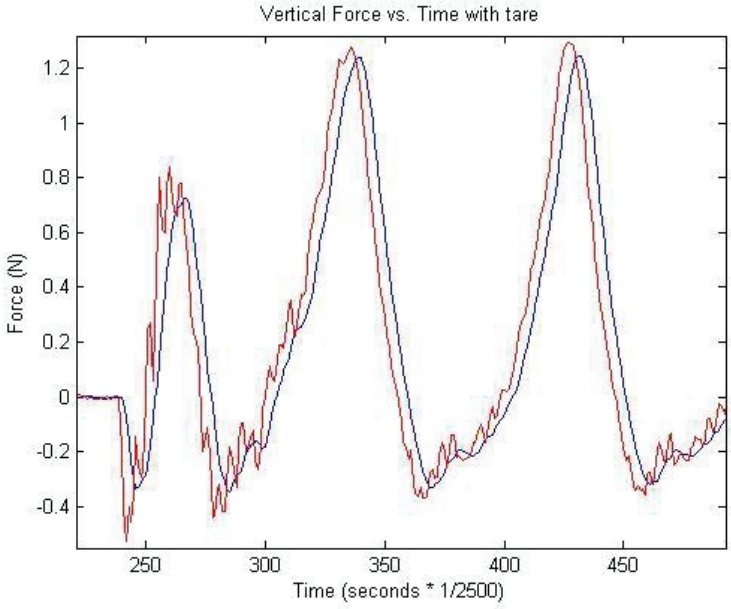

Figure 10: Unfiltered response (red), Filtered response (blue)

4.6 Signal Processing

The signal processing comprised of three parts, two of which will be discussed here. These two are image tracking and implementing the post-processing low-pass filter. It was pointed out in the theory section that there are three parameters that are necessary in order to mechanically compute the power of a system, and they are force, displacement, and time. The force data is directly output from the signal communications code that executes the shaker movement and camera triggering.

From here, the displacement of the shaker and linkage system is the next parameter necessary for the power computation. The displacement data for the shaker is back calculated from the images taken by the high speed camera. The images for a single run would be saved to an individual folder where the tracking code would be placed and ran. The point(s) tracking code was modified from a code written by Murray [7], which was written to track up to a dozen points along a flapping *Manduca* wing. The code works by computing a normalized cross correlation between one image and the next, looking for the originally selected sub-image which should have moved only a few pixels between frames. In the case of the current experiment, the only pertinent motion to track was the vertical translation of the shaker, so only one sub-image was selected. A distinct shape with clear lines was found to be the most reliable tracking target, as shown in Figure 9. The program tracks the selected points in terms of pixel location in the image, therefore there is a need to convert that pixel location to a meaningful value. The originating pixel was set to a zero location and any variance off of that registered pixel indicated either a positive or negative value which was then converted to mm through a pixel to mm conversion factor. This factor typically remained constant for all test runs; the only way this value would change is if the camera was moved.

The next segment of the code uses a built in MatLab function to create a movie file of the acquired images. The coordinates of the tracked point were superimposed, in the form of a red plus, on the images for the movie file, allowing the tracked point to be shown as the movie plays. This helped indicate any oddities in the displacement data. Lastly, the script creates displacement arrays for both the shaker and the longitudinal motion of the pivot.

Considering the linkage kinematics, in order to solve for the displacement of interest one variable is necessary, the crank angle, however in order to obtain that value it can either be visually captured from the images or back calculated from the vertical displacement of the shaker. Three values are necessary to obtain the crank angle, slider displacement, and the linkage arm lengths. The arm lengths are fixed based on the design and the slider displacement was computed in the above code segment. In order to calibrate the pivot displacement from its initial starting point, the initial crank angle was required. This was determined by manually measuring the angle of the crank from the camera images during the tare period. With the starting point of the linkage system and the vertical displacement of the shaker known, the angle can be computed from the vertical displacement and therefore the horizontal displacement of the pivot is calculated. The values of displacement are again centered on the starting point of the system. A negative pivot displacement corresponds to movement toward the specimen. The units of the angle are in radians and the lengths and displacements are in mm.

For the power calculation processing, when the force data was filtered an added known phase shift occurred and to ensure the force and displacement data matched up, frame for frame, the displacement data was filtered as well (producing mainly just a phase shift of the data).

4.7 Power Calculation

In order to calculate the mechanical power output: force, displacement, and time are necessary, the first step to computing the power was to determine where contact began on the tergum and phragma and when the corresponding compression ended. This was determined by analyzing the force and displacement data and the camera images. The first flap forces are typically low in amplitude as the system is approaching steady state for the first couple flaps so the first flap is ignored for power considerations.

An example single flap force and displacement data set for an upstroke and downstroke is shown in Figure 13. Next, the work and power are computed. The work is numerically integrated by using a built in MatLab function *trapz*, the integration is of the force over with the displacement being the limits. Lastly, the power is computed by taking the work value and dividing it by the time interval that the work occurred over. All of the displacement, time, work, and power values are saved to respective arrays containing the information for all 24 flaps. The power is then averaged over the series of flaps to get an average power to perform the respective motion, upstroke or downstroke. The ability to

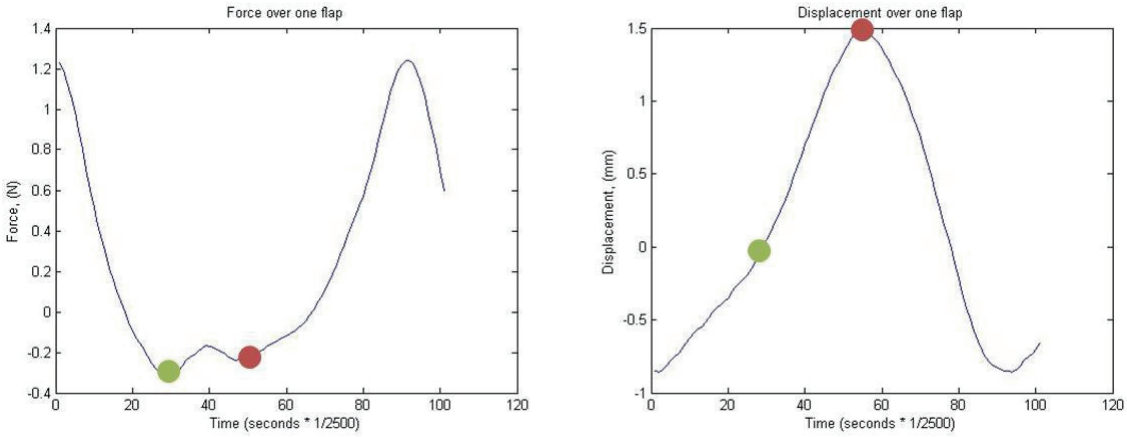

Figure 11: The range of force and displacement from green to red (grey to black) for the upstroke.

compute all of those variables for each individual flap allows for a more in depth power analysis for the full flapping stroke. The important trends that were searched for during the analysis of all of the flaps were consistency and overall repeatable data from flap to flap. A close up view of a force vs. displacement chart for the vertical and longitudinal motion is shown in Figure 11 and Figure 12.

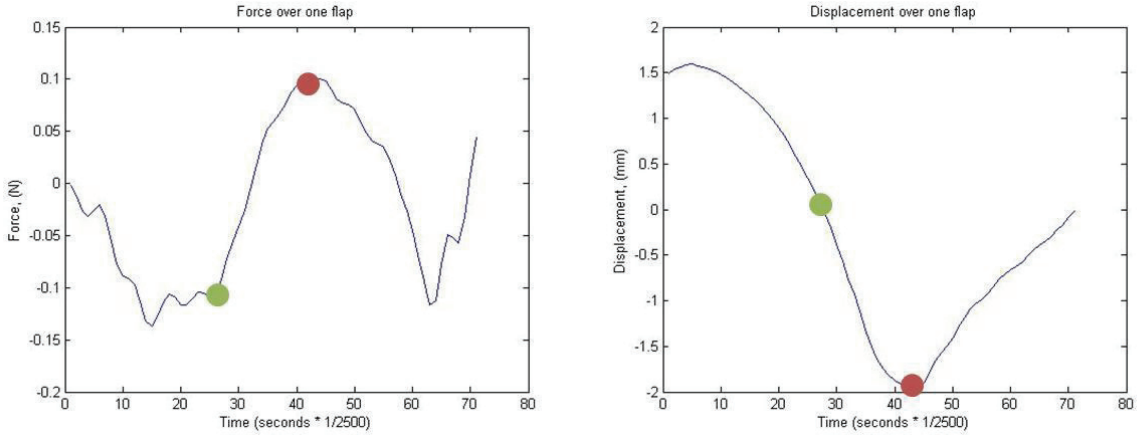

Figure 12: The range of force and displacement from green to red (grey to black) for the downstroke.

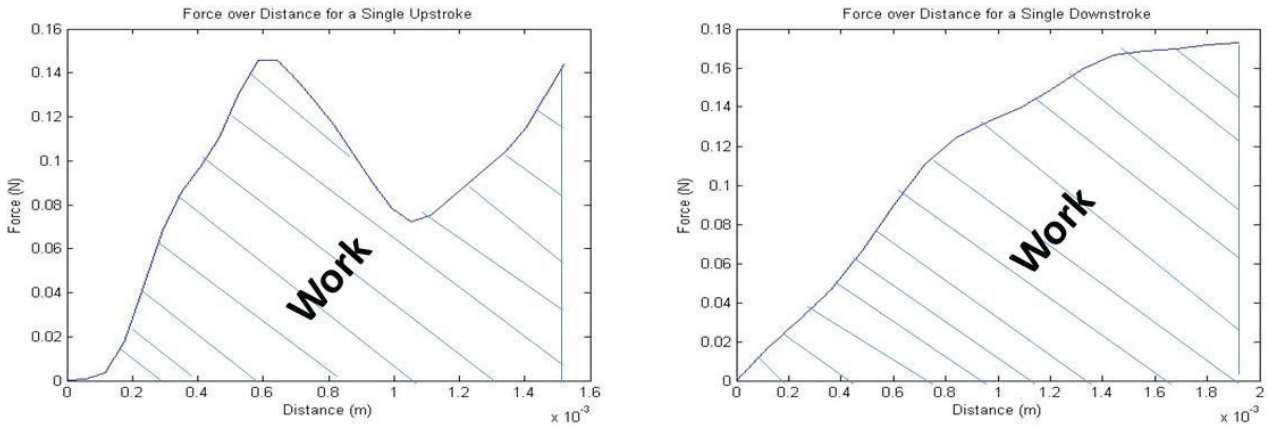

Figure 13: Close-up view of the Force vs. Displacement for the upstroke (right) and the downstroke (right).

5. RESULTS AND DISCUSSION

The modified dynamic load experiment was implemented to simultaneously determine the power output of the DVM's and DLM's for 5 *Manduca sexta* specimens. The average mechanical power required to produce the upstroke and downstroke replicating the natural flapping motion of the *M. sexta* was found to be 13.34 ± 1.08 mW and 31.36 ± 2.55 mW respectively totaling to 44.92 mW. The respective flap angles for the power results were calculated based on the trigonometry relationship to be a 60 deg upstroke and a 35 deg downstroke. These values were confirmed to be the flap amplitudes observed by the *Manduca* in nature during hovering flight as shown by the work performed by Guiler. The results provided for displacement, time, work, and power are all averages of flap number 15-25 in Table 2 and Table 3. The average was taken at this point because this is where steady-state flapping was determined to occur for most cases. Frequently, but not observed in all wings cases the absolute power for the upstroke was initially large and as the flaps continued the power decreased by approximately half to a steady state value. This is shown in Figure 15. Let it be noted that for this test and others that observed this trend the force vs. displacement plots for all flaps were nearly identical in trend, only the amplitudes lessened as flaps progressed. The resulting power array could have many implications such as, a settling time for the moth to reach steady state flapping, the initial flaps are the most energy demanding and require an energy density of approximately 216 W/kg (roughly double what is required for steady state flapping (112 W/kg)), and elastic energy storage of the thorax as it becomes energized. On the other hand, all of the no-wings cases did not display this trend and had more consistent absolute power measurements spanning all flaps. This is shown in Figure 16 and Figure 17. Another point of interest that was observed was that the absolute power required for the no-wings case equals approximately the settled steady state value of that reached for the with-wings cases. If the assumption is made that the steady with-wings case and no-wings case produce approximately equal values of absolute power, which was observed, then combining the resulting power data would be justified. The resulting charts shown in Table 2 and Table 3 do combine the with-wings cases and no-wings cases for an averaged absolute power required for the upstroke and downstroke. The force values recorded for all of the moths tested were quantifiably repeatable for each moth respectively as long as once the moth was placed in the apparatus it was not adjusted between successive tests. The placement of the moth in the apparatus had significant effects on the power results and precise alignment needed to be performed to ensure the pushrods were pushing on the correct points along the tergum and phragma alike. These points were specific to coincide with where the muscles attached to the tergum and phragma.

Through high speed video observations and load data correlation, there is evidence that there exists elastic storage of inertial energy. This is particularly evident during the with-wings testing. When the thorax is loaded and unloaded its skeletal structure reacts like a spring within the system with the ability to store and release energy. The storing of the energy is due the contraction of the spring-like structure of the thorax. Through video observation, it was seen that the wings moved though intermediary positions of the wing stroke even though there was no movement of the thorax due to compression. With every stroke, the compression for the vertical direction would take approximately 10 ms and the longitudinal direction was approximately 5 ms, the moth flaps at approximately 28 Hz meaning 35 ms per flap, if the muscle actuation is only for 15 ms out of the 35 ms and wing displacement is occurring over the 35 ms then there is work being done by the structure on the wings which is due to the elastic inertial stored energy. This is shown in Figure 14.

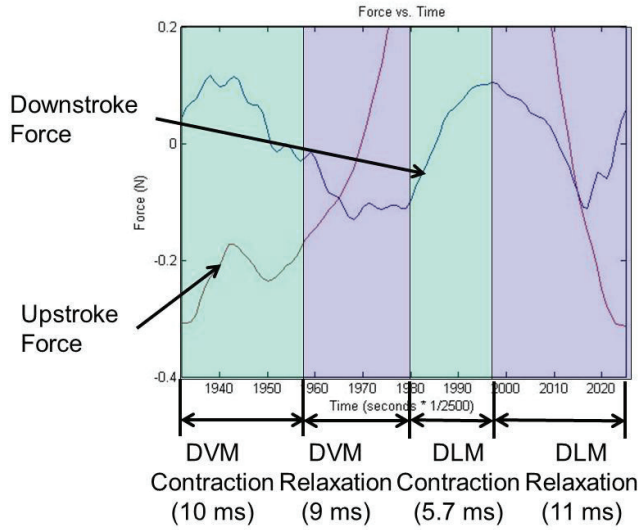

Figure 14: Time plot depicting the individual segments of an entire flapping sequence.

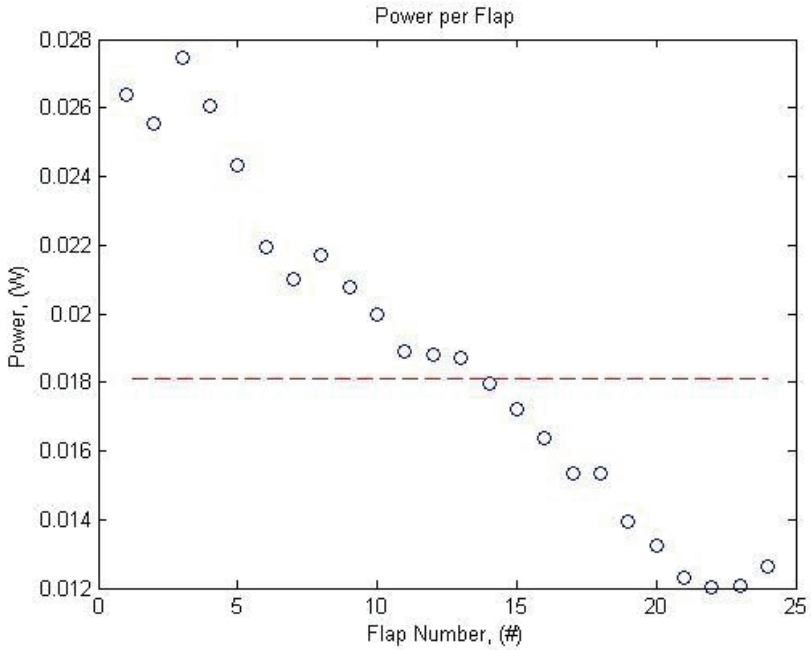

Figure 15: Absolute Power per Flap for upstroke for specimen 3 with-wings specimen test (red dashed line is the average for last 15 flaps)

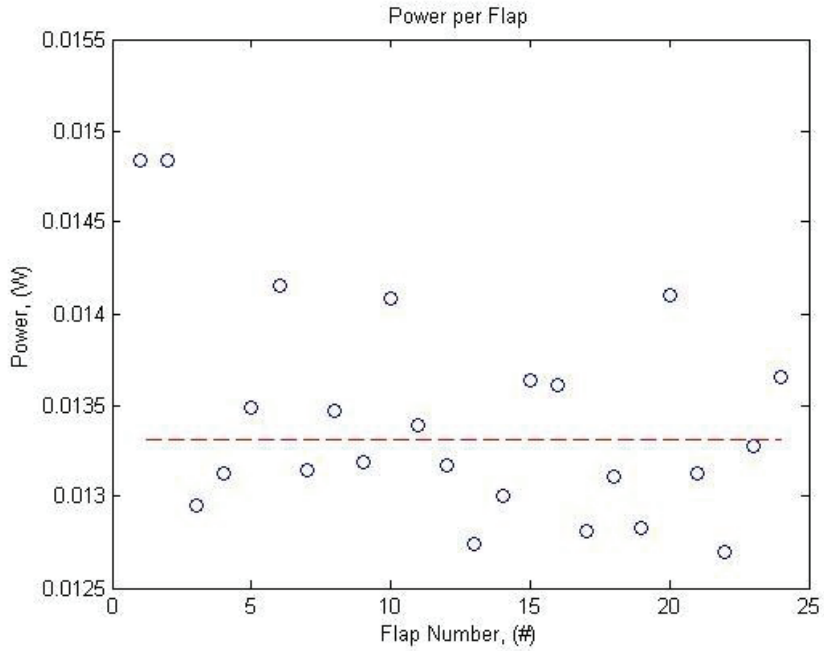

Figure 16: Absolute Power per Flap for upstroke for specimen 4 with no-wings specimen test (red dashed line is the average for last 15 flaps)

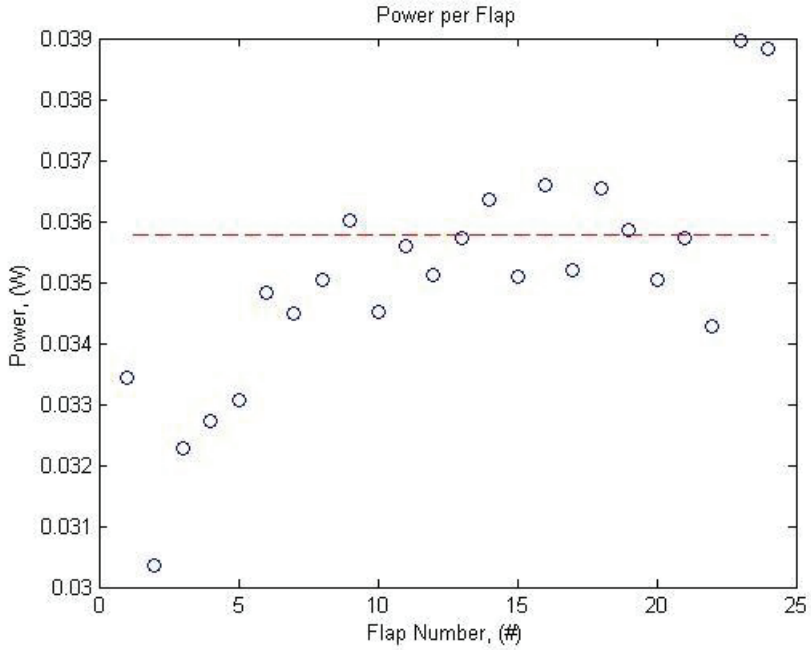

Figure 17: Absolute Power per Flap for downstroke for specimen 4 with no-wings specimen test (red dashed line is the average for last 15 flaps)

Table 2 : Upstroke Power Data for the 5 test specimens.

Upstroke Power Data							
Specimen	Date	Mass (g)	Disp (mm)	Time (ms)	Work (J) x10^{-4}	Power (mw)	Wings Present
1	10/17/2012	1.74	1.16	9.3	1.42	15	yes
2	10/18/2012	1.82	0.78	7.6	1.12	14.5	yes
3	11/5/2012	1.95	1.56	10.5	1.27	12	yes
4	11/12/2012	1.85	1.47	10.2	1.37	13.3	no
5	11/14/2012	1.7	1.5	10.3	1.34	13	no
Average		1.81	1.29	9.58	1.30	13.56	
St.Dev		0.10	0.33	1.20	0.12	1.20	

Table 3 : Downstroke Power Data for the 5 test specimens.

Downstroke Power Data							
Specimen	Date	Mass (g)	Disp (mm)	Time (ms)	Work (J) x10^{-4}	Power (mw)	Wings Present
1	10/17/2012	1.74	1.44	4.8	1.45	30.7	yes
2	10/18/2012	1.82	1.41	5.9	1.82	31	yes
3	11/5/2012	1.95	1.79	5.6	1.61	28.5	yes
4	11/12/2012	1.85	1.94	6.4	2.25	35.5	no
5	11/14/2012	1.7	1.94	5.8	1.8	31.1	no
Average		1.81	1.70	5.70	1.79	31.36	
St.Dev		0.10	0.26	0.58	0.30	2.55	

The value of power obtained here is the absolute power required for these muscle groups to accomplish the respective wing movements. In order for comparison to other muscular groups and energy storage systems, the absolute power is divided by the mass of the working unit. In this case, the absolute power per stroke will be divided by their respective mass percentage of muscle. This term is referred to as the specific power density. For the purposes of the research, the moth's muscles were not extracted and weighed because the dissection skills necessary were outside the scope of this project. However, extensive research was performed on mass percentages of the various segments of the *Manduca*. The documentation detailed by Willmott and Ellington presents that an average muscle mass to body mass percentage is 27 percent for males and 17.7 percent for females [8]. An average of this value was taken for the purposes of the research to estimate a specific power density of the DVMs and DLMs. Figure 18 displays a chart plotting the specific power density of the DVMs, DLMs, and the combination of the two. The plot depicts both the DVM and DLM mass percentages varying with respect to each other. For instance if the DVM's equal 15% of the muscle mass then the DLM's would equal the remaining 85%. The assumed muscle mass was derived from Willmott's and Ellington's experiments to be 22% of the overall moth weight. The upstroke and downstroke data presented above correspond to the DVM and DLM muscle groups respectively. The value of power used in the calculation of the specific power density was the average of all of the specimens, 13.34 mW and 31.36 mW respectively. In varying the muscle mass percentages it was found that there is a ratio of DVM to DLM that equates to an equal specific power density between the two. This was approximately 30% DVM to 70% DLM muscle mass equaling the value of 112 W/kg muscle. This point lies where the red and blue line intersect in Figure 18. It is expected that such a value should exist because both sets of muscles are composed of the same muscle tissue therefore they should have the same specific power density. The hawkmoth in nature exhibits muscle mass ratios of the order presented (30/70) therefore confirming what was found to be the muscle mass ratio which yielded an equal power density. The total power density was also plotted with respect to varying the total muscle mass percentage which was assumed to be 22% for the red and blue lines. (15-40%). Here the ratio of DVM to DLM was fixed at 30% to 70% respectively. This value analyzed over the muscle mass range that Willmott presented produces specific power density values of 140-91 W/kg muscle. Figure 19 contains a table with the specific power density values presented in the literature review and from a few other sources to compare these values with those developed by the experiment and technique presented.

This experiment yielded a power density which lies very close to the bulk of the accepted data presented. The most reliable results involve those that experimented directly with the specimen or muscles themselves. These were the work presented by Pennycuick, Stevenson and Josephson, and Tu [11], [12], [5]. Their results fell within the range of 82-97 W/kg muscle. The other experiments values are less reliable as applied to muscles themselves because they obtain the power value indirectly with computational or numerical models and equations. In order to do this, the models typically require numerous assumptions and simplifications which make the results less reliable. One experiment in particular that yielded a value that is indeed high was Casey's prediction [1]. The main cause of the overestimation was the use of the 20% efficiency factor for the muscles. It has since been shown by Josephson and Tu that this value lies more in the range of 5-10% which drives Casey's estimate to 102-135 W/kg muscle mass. Using the now more accepted value for the muscle efficiency Casey's estimates fall within the rest of the presented results. These values particularly fall exactly within the results of the dynamic load experiment.

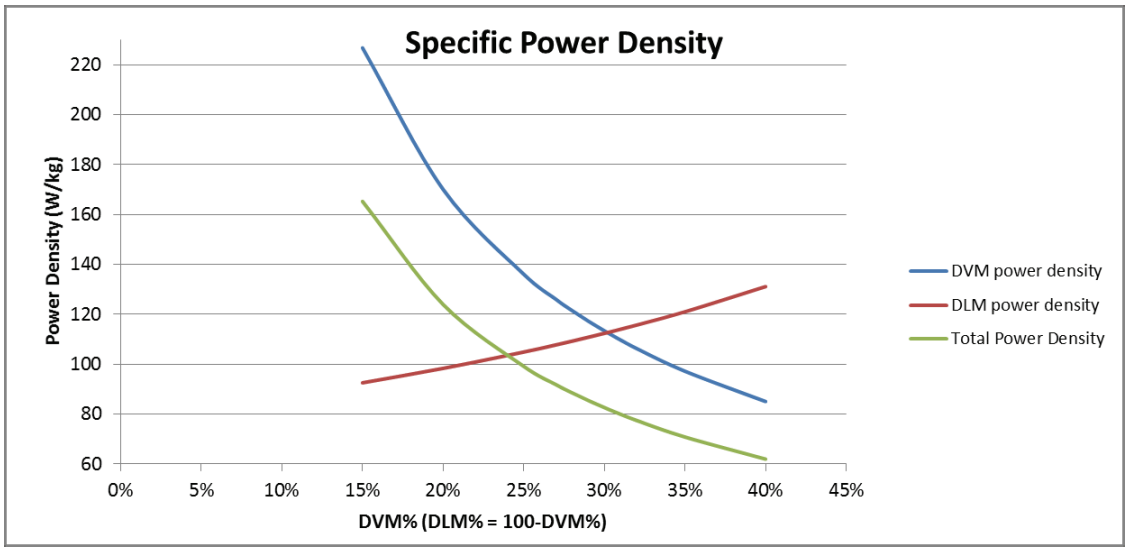

Figure 18: Specific power density of the DVM's and DLM's ranging in percentage density and Total power density ranging in total muscle mass weight percentage.

In addition, future work built off of Ryan O'Hara's flapper has been performed by Anthony Deluca in order to characterize the power required by the piezoelectric system to reproduce the full flapping stoke of a man made wing/actuator system [10]. The power required for one wing was found to be approximately 100 mW to produce a flap stroke of 90 deg. This value compared to the power obtained by mechanically compressing the thorax (50mW) is approximately four times the amount seen in this research work. This is true if you assume that the 100mW of power is necessary to flap each wing independently which would yield a total power of 200mW compared to 50mW for the thoracic study. The man-made flapper appears to require more power to flap the "same" wing. A potential reason for the flapper requiring more power could be possible inefficiencies in its piezoelectric linkage actuator.

Figure 19: Specific power output from the various sources in the literature review. Specific power density comparison chart.

***M.sexta* Power Output**		**specific power ($W*kg^{-1}$)**		
researcher/year	**method**	**body mass**	**muscle mass**	**notes**
Casey 1976	estimation from power input	41-54	***205-270**	Based on measurements of power input and estimate of 20% efficiency. We now know that actual efficiency is much lower
Pennycuick, Rezende 1983	muscle study	-	82-97	Estimated power density of muscle based on a known value for power density of mitochondria
Stevenson, Josephson 1990	work-loop	-	90	Mean maximum power. Absolue max reached 130 in two specimens. 50-80 determined to be min. power req'd for flight
Sun, Du 2003	numerical	33-39	***164-194**	With elastic storage - without elastic storage
Tu, Daniel 2004	work-loop	-	83.3	Specifically studied the DLMs
Liu, Aono 2009	computational	39.5	***197.5**	Diff. species of hawkmoth, *Agrius convolvuli*
Zhao, Deng 2009	kinematics and aerodynamics	19.7 (aero) 16.4 (inertial)	***98-180**	With elastic storage (no inertial power) - Without elastic storage (must overcome all power requirements)
Hollenbeck 2012	mechanical	-	†**72-143**	Direct measurement of mechanical power
Cranston, 2012	mechanical		****112**	Direct measurement of mechanical power for both DVM and DLM flight muscle groups
*indicates equivalent value based on 20% muscle mass			†estimated range based on DVM/flight muscle ratio of 15% - 30%	
**30% DVM 70%DLM				

***M.sexta* Power Input**		**specific power ($W*kg^{-1}$)**		
researcher/year	**method**	**body mass**	**muscle mass**	**notes**
Casey 1976 (Reporting Heinrich 1971)	metabolic	191-289	478-722	Moth flies in closed jar and depletion of oxygen is measured/correlated to energy by
Casey 1976	metabolic	237	694	Based on oxygen consumption
Stevenson, Joesephson 1990	metabolic	-	**1170**	Derived from Heinrich's 0_2 consumption. Most reliable number based on newer data

5.1 Results Summary

The dynamic load experiment reproduced the entre wing stoke replicating hovering in the *M.sexta* while measuring the absolute power required to reproduce the wing motion. The absolute value was associated to the individual flight muscle groups and as an entire mass of unity. The results of this experiment were in agreement with other research presented on the measured mechanical specific power density of the *M.sexta* flight muscles. The value of specific power density found was to be 112 W/kg at a 70/30 ratio of DLM to DVM muscle mass percentage.

6. CONCLUSIONS

The dynamic load apparatus is the one of its kind to mechanically compresses the thorax in such a manner that the wings travel through their full range of motion. This technique allows for testing of the specimen with all natural boundary conditions intact. All other techniques used required the muscle fibers to be partially or fully removed for instrumentation and experimentation. Sources of error can arise from adhesion of the muscles to the stretch rod and not having exact exoskeleton material to adhere to.

The absolute power of the dorsoventral and dorsolongitudinal muscles as presented was 13.3 and 31 mW. If the assumption is made that both muscles groups are of the same biological composition then

the specific power density of the muscular tissue must be a single value. This would then require that the DVMs and DLMs have the same power density. In varying the weight percentage of both muscle groups it was shown in Figure 18 that the point where both are equal to each other is 112 W/kg at 70% DLM and 30%DVM of the total muscle mass. This being true, implies that the muscle mass ratio within the thorax is 70% DLM to 30% DVM.

In looking to create an actuator wing combination the actuator needs to be light enough to lift and provide enough force to lift the vehicle. This combination of constraints makes creating an actuator wing combination difficult because typically power is directly proportional to the mass of the object or material in an increasing fashion. The work performed here has produced a baseline for what should be targeted for in design of an actuator and wing mechanism. With reference to the hawk moth, the specific power density of the vehicle itself is 2.5 mW/kg or 44 mW/1.8kg. This encompasses the actuator, wings, and power source for the *M.sexta*. This value would be a baseline for what to target for on the design of a FWMAV actuator, wing, and power source system. One actuator type in particular that is being researched heavily and has seen itself on FWMAV's is a piezoelectric actuator which can have energy densities as high as 400 W/kg.

Harvard has been able to utilize these actuators to produce a flying fly yet the power source of the vehicle is tethered to the vehicle, therefore not complete free flight. The set back at the moment is in the development of power sources that are light and energy dense enough to be carried by FWMAVs.

7. ACKNOWLEDGEMENTS

The authors would like to thank Dr. Doug Smith of the Air Force Office of Scientific Research for his oversight and support. The views expressed in this article are those of the authors and do not reflect the official policy or position of the United States Air Force, Department of Defense, or the U.S. Government.

REFERENCES

[1] T. Casey, "Flight Energetics of Sphinx Moths: Power Input During Hovering Flight," *Journal of Experimental Biology,* vol. 64, pp. 529-543, 1976.

[2] M. A. Frye, "Effects of stretch receptor ablation on the optomotor control of lift in the hawkmoth Manduca sexta," *The Journal of Experimental Biology,* pp. 3683-3691, 2001.

[3] C. Bolsman, "Flapping Wing Actuation Using Resonant Compliant Mechanisms," Ipskamp, ISBN 9789090256856, The Netherlands, 2010.

[4] R. F. Chapman, The Insects, 4th edition, Cambridge: University Press, 1998.

[5] M. S. Tu and T. L. Daniel, "Submaximal power output from the dorsolongitudinal flight muscles of the hawkmoth Manduca sexta," *The Journal of Experimental Biology,* pp. 4651-4662, 2004.

[6] A. Slocum, "Fundamentals of Design: Linkages," 12 Dec 2008. [Online]. Available: http://web.mit.edu/2.75/resources/FUNdaMENTALs%20Book%20pdf/FUNdaMENTALs%20Topic%204.PDF. [Accessed 05 Oct 2012].

[7] J. Murray, R. O'Hara and A. Palazotto, "The Use of Photogrammetry to Evaluate Dynamic Characteristics of a Manduca Sexta Wing," in *Dayton Engineering Sciences Symposium (DESS)*, Dayton, 2011.

[8] A. Willmott and C. Ellington, "The Mechanics of Flight in the Hawkmoth Manduca Sexta," *Journal of Experimental Biology,* vol. 200, pp. 2705-2722, 1997.

[9] A. C. Hollenbeck, "Evaluation of the thorax of manduca sexta for flapping wing mirco air vehicle applications," Air Force Institute of Technology, Dayton, 2011.

[10] A. M. Deluca, M. F. Reeder and R. G. Cobb, "An Experimental Investigation into the Effect of FLap Angles for a Piezo-Driven Wing," *International Journal of Micro Air Vehicles,* vol. 5, no. 1, pp. 55-92, 2013.

[11] R. Stevenson and R. Josephson, "Effects of Operating Frequency and Temperature on Mechanical Power Output form Moth Flight Muscle," *Journal of Experimental Biology,* vol. 149, pp. 61-78, 1990.

[12] C. Pennycuick and M. Rezende, "The Specific Power Output of Aerobic Muscle Related to the Power Density of Mitochondria," *Journal of Experimental Biology,* vol. 108, pp. 377-392, 1984.

[13] B. Cranston, "EVALUATION OF THE THORAX OF THE MANDUCA SEXTA FOR FLAPPING," 03 2012. [Online]. Available: http://www.dtic.mil/dtic/tr/fulltext/u2/a574287.pdf. [Accessed 28 04 2014].